Int. J. Electrochem. Sci., 7 **(2012)** 8487 - 8502

International Journal of
ELECTROCHEMICAL
SCIENCE
www.electrochemsci.org

Susceptibility to Stress Corrosion Cracking and Electrochemical Behavior of Electroless Ni-P /nano-TiO_2 Composite Coatings on 70-30 Brass in Fluoride Solutions

Cheng- Kuo Lee[1,*]

Department of Mechanical Engineering, Chien Hsin University of Science and Technolog, Chung-Li, Taiwan 32097, R.O.C.
[*]E-mail: cklee@cyu.edu.tw; (will be changed as cklee@uch.edu.tw on Aug. 01, 2012)

Received: 12 July 2012 / *Accepted:* 31 July 2012 / *Published:* 1 September 2012

In this investigation, electroless plating techniques were utilized to form Ni-P/nano-TiO_2 composite coatings on a 70-30 brass alloy substrate by adding nano-TiO_2 to the Ni-P plating solution in concentrations of 1 g/L, 5 g/L, 10 g/L and 15 g/L. The electrochemical corrosion resistance behavior of these composite coatings and their susceptibility to stress corrosion cracking (SCC), which were related to their surface morphology and microstructure were studied by comparing them with those of an Ni-P coating. Experimental results revealed that the electroless Ni-P plating coating increased the hardness and the resistance to corrosion and SCC of the brass alloy in 0.1 M NaF solution. When nano-TiO_2 particles were added, this beneficial effect increased significantly with their concentration up to 15 g/L. The improved SCC resistance was attributed to the electroless Ni-P/nano-TiO_2 composite coatings, which prevented the formation of an unstable Cu_2O passive film on brass alloy in fluoride solution. This unstable passive film was destroyed by tensile strain and F^- attack during tensile testing with slow strain in fluoride solution, resulting in dezincification dissolution and intergranular stress corrosion cracking (IGSCC) of the brass alloy.

Keywords: TiO_2 ; SCC; Electrochemical; Corrosion ; IGSCC.

1. INTRODUCTION

Whether a brass alloy exhibits good or poor cold working behaviour depend on the amount of Zn that it contains. Typically, brass alloys with a low Zn content have good or excellent cold working characteristics, while those with a high Zn content have poor cold working characteristics. Brass alloys are most frequently used to fabricate condenser and heat exchanger tubes with integral fins on which

the external and/or external surfaces have had their in-service efficiency enhanced by cold work finishing. Generally, cold working operations cause internal stresses, which can result in stress corrosion cracking (SCC). Ammonia and ammonium compound [1,2], nitrite [3,4], chloride [5] and fluoride [6-9] ions are strong promoters of SCC in α-brass in service environments.

In the last decade, the SCC of brass alloys has been prevented in two ways. The first is by using an alloy with high resistance to this phenomenon (an alloy with a low Zn content) and the other is by reducing residual stresses by annealing. This heat treatment, which is commonly carried out at approximately 250˚C, is also performed to minimize the distortion that may occur during machining. This low temperature heat treatment is also known as "stress-relief annealing", and does not influence the mechanical properties of the material.

Shih et al. [8,9] recently performed a study to evaluate the effect of such inhibitors as 1,2,3-benzotriazole (BTA) and 1,2,4-triazole in suppressing the SCC of 70-30 brass in chloride and fluoride environments. Their study included an analysis of the fracture surfaces of the tested specimens using SEM techniques and the plotting of electrochemical polarization curves in NaCl and NaF solutions, with and without inhibiting triazole derivatives. Their results revealed that the studied corrosion inhibitors reduced the susceptibility of the brass alloy to stress corrosion cracking, particularly in the early stage of crack propagation. The effects of pH and such electrochemical parameters as pitting and protection potential on the SCC of brass in fluoride solutions have been elucidated [6].

Most components are well known to fail because of surface defects that are caused by wear, corrosion, fatigue or fracture, for example [10]. The surfaces of components are coated to improve their surface properties. Brass alloys, aluminum alloys, magnesium alloys, steels and other nonmetals are suited to electroless nickel (EN) plating. Such coatings improve the hardness, wear, abrasion resistance, and corrosion resistance of these materials [11-15]. In the chemical, mechanical, automobile and electronic industries in particular, electroless Ni-P coating has been utilized extensively for coating alloy components to improve their inherent characteristics. An interesting feature of electroless Ni-P coatings that are deposited on aluminum substrates is that the P content of the deposit may make the residual stresses compressive [16], improving the fatigue performance of the coated system. Parker and Shah [16] found that in as-deposited electroless Ni–P-coated aluminum substrates, the residual stresses in the deposit fall linearly as the P content of the coating increases, from approximately 10 MPa for coatings with 2 wt% P to approximately -60 MPa for coatings with approximately 12 wt% P. Additionally, an electroless Ni-P coating can be doped with various particulates to fabricate novel multifunctional composite materials. For example, the introduction of hard particles, such as nano-TiO_2 into an electroless Ni-P alloy coating has been found to improve its mechanical and physical properties [17-19]. However, the literature has not discussed the electroless nickel (EN) plating of brass alloys to inhibit corrosion and SCC susceptibility in fluoride environments.

The goal of this study is to examine the effects of the addition of TiO_2 in the electroless Ni-P coating on the electrochemical and SCC behavior of 70-30 brass alloy substrate in 0.1 M NaF solutions by performing slow strain rate tensile (SSRT) tests. Electroless Ni-P/nano-TiO_2 composite coatings were carried out on the brass by adding various concentrations of nano-TiO_2 particles (with an average diameter of approximately 15 nm) to the Ni-P plating solution. The coating was compared with the Ni-P coating without added nanoparticles. A method is introduced for evaluating the ability of these

coatings to protect the brass alloy based on the results of the electrochemical and SCC tests. The structure of the coatings is analyzed to elucidate the mechanism and to identify the composite coating with the optimal nano-TiO_2 content.

2. EXPERIMENTAL

The material that was utilized in this study was 70-30 brass UNS C26000, which has the chemical composition (wt.%) :68.5~69.0% Cu, Pb ≤ 0.03%, Fe ≤ 0.03%, and balance Zn. Electrochemical measurements were made of a rectangular sample with a 1.5 cm × 1.5 cm × 0.5 cm. Cylindrical SCC specimens were machined to 54.0 mm long and 4.82 mm in diameter, they were threaded on both ends to facilitate attachment to the pulling device. The gauge section was 3.22 mm in diameter and 15.0 mm long, and was fabricated according to ASTM G49-85 [20]. Samples were then ground using 400, 600, 800 and 1200 grit silicon carbide (SiC) abrasive paper and polished using 1 μm and 0.3 μm Al_2O_3 powder pastes to prevent any possible notch effects. The pretreatment procedure involved ultransonic cleaning in acetone for 5 min, washing in a 50 g/L NaOH solution for 3 min and etching using a 300 g/L HNO_3 solution for 1 min at room temperature (~25 ˚C). Between steps each specimen was rinsed by immersion in distilled water at room temperature for 2 min. All specimens were then immersed in the Ni-P plating solution at 85 ± 1 ˚C. The Ni-P electroless plating solution comprised 35 g/L $NiSO_4 \cdot 6H_2O$, 50 g/L $Na_3C_6H_5O_7 \cdot 2H_2O$, 20 g/L $NaH_2PO_2 \cdot H_2O$, 5 g/L $CH_3COONa \cdot 3H_2O$, 40 g/L NH_4Cl and an additive at pH 4.6. Titanium dioxide (TiO_2) nanopartcles with an average diameter of 15 nm were added to the plating solution at concentrations of 1, 5, 10 and 15 g/L for codeposition to form the composite coatings. During electroless deposition for 60 min, to minimize the agglomeration of TiO_2, the plating solution was ultrasonically dispersed for 15 min, and magnetically stirred at a constant speed of 100 rpm. The microhardness of the coating was measured using a Vickers microhardness tester (MHT 2) at a load of 100 g for 15 s. Surfaces and cross-sections of the coatings were studied by scanning electron microscopy (SEM, JEOL JSM-6360) and X-ray energy dispersive spectrometry (EDS, INCA Energy 6587).

Electrochemical polarization tests were performed on the electroless composite coatings on 70-30 brass substrate in 0.1 M NaF solution using a potentionstat/galvanostat (Model 273A, EG & G Instruments, USA) with a three-electrode cell with an exposed area of 1 cm^2. All potentials referred to a saturated calomel electrode (S.C.E.). A platinum wire was used as the counter electrode. The potentiodynamic polarization curves were scanned from 0.25 V_{SCE} below OCP to a final potential of 1.2 V_{SCE}, at a sweeping rate of $1mV \cdot s^{-1}$. A Tafel-type fitting of the data was performed using EC-Lab sofware to estimate the corrosion rate (i_{corr}) and the polarization resistance (R_p). The five tests were carried out for each coated sample to evaluate reproducibility.

Slow strain rate tensile (SSRT) tests were performed under the open-circuit condition in 0.1 M NaF solution. SSRT tests are regarded as advanced SCC tests because they yield certain results in a period that is much shorter than that required to perform the conventional constant-deformation or constant-load SCC tests [21]. The use of SSRT tests in evaluating the SCC susceptibility of brass alloys in a wide range of environments is widely acknowledged to be effective [6-9]. In this study, the

test specimen was passed through silicon rubber stoppers that were fitted at each end of a cylindrical glass test cell (with a volume of 200 mL) containing the test solution. The load and elongation were measured continuously using a load cell and electrical dial gauge, respectively, whose outputs were recorded on a computer using control software until fracture occurred. *Bradford et al.* [22,23] found that in various SCC-inducing environments, cracking occurs in copper alloys only below a particular strain rate (10^{-4} s^{-1}) and, therefore, a strain rate of 2.22×10^{-7} was used to the specimen herein this study. Following SSRT testing, the fracture surfaces and fracture modes of SCC were analyzed by SEM.

3. RESULTS AND DISCUSSION

3.1. Characterization of coatings

Figure 1 presents SEM images of the surface morphology and elemental composition of the electroless Ni-P coating. Figure 1a reveals that the surface morphology of the Ni-P coating is a smooth and the structure is dense with very small spherical nodular particles. Although the 70-30 brass is less noble than the Ni-P coating, the smooth coating suggests the better protectiveness of the Ni-P coating. EDS analysis of the coating surface yields strong Ni and P signals (Fig. 1b). The P content in the elemental analysis is as high as 20.03 wt.%, and the Ni-P coating is probably amorphous [24]. Generally, amorphous alloys have higher corrosion resistance than equivalent polycrystalline materials because they have no grains and grain boundaries [25].

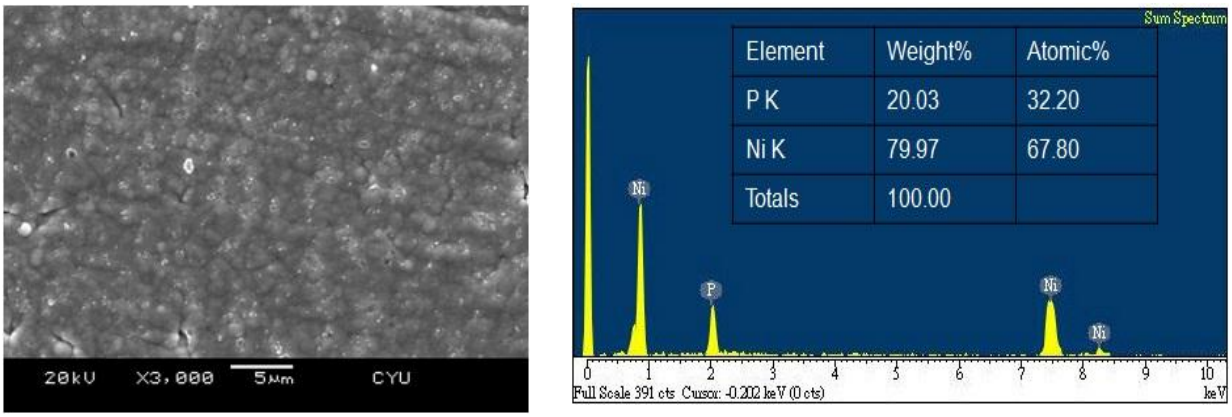

A **B**

Figure 1. (a) SEM surface morphology and (b) EDS elemental analysis of electroless Ni-P coating.

Figure 2 presents SEM images of the surface morphology of the Ni-P/nano-TiO_2 composite coatings formed by adding 1, 5, 10 and 15 g/L TiO_2 nanoparticles to the Ni-P plating solution. The Ni-P/nano-TiO_2 composite coating formed by the addition of 1 g /L TiO_2 nanoparticles showed no

nodular particles and a finer and more continuous structure than that of the Ni-P coating (Fig. 2a). When the concentration of TiO_2 nanoparticles was increased to 5 and 10 g/L, the formed Ni-P/nano-TiO_2 composite coatings were more continuous, smoother and denser, and more small, white spherical particles were codeposited, while the distribution remained uniformly (Figs. 2b, 2c). However, when the concentration of TiO_2 nanoparticles was further increased to 15 g/L, the aggregation of the white, small spherical particles increased, and the formed composite coating became rough with exhibiting many small cracks indicated by arrows (Fig. 2d).

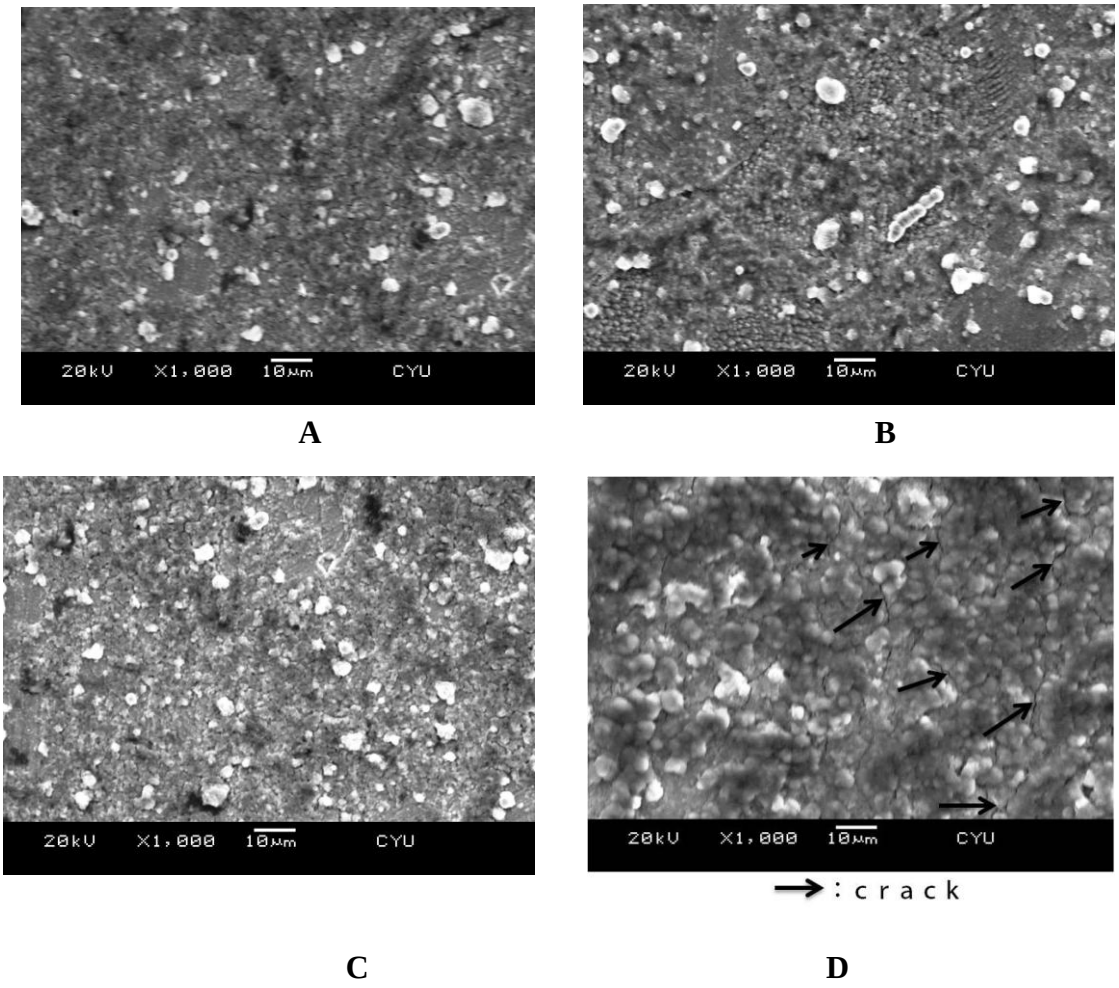

Figure 2. SEM surface morphology of electroless Ni-P/nano-TiO_2 composite coatings: (a) N-P/1 g/L TiO_2, (b) N-P/5 g/L TiO_2, (c) N-P/10 g/L TiO_2 and (d) N-P/15 g/L TiO_2.

Figure 3a presents an SEM image of the surface morphology of the N-P/nano-TiO_2 composite coating that was formed at a TiO_2 concentration of 10 g/L. O and Ti were uniformly distributed throughout the surface, although agglomeration was observed in some places (Figs. 3b and 3c).

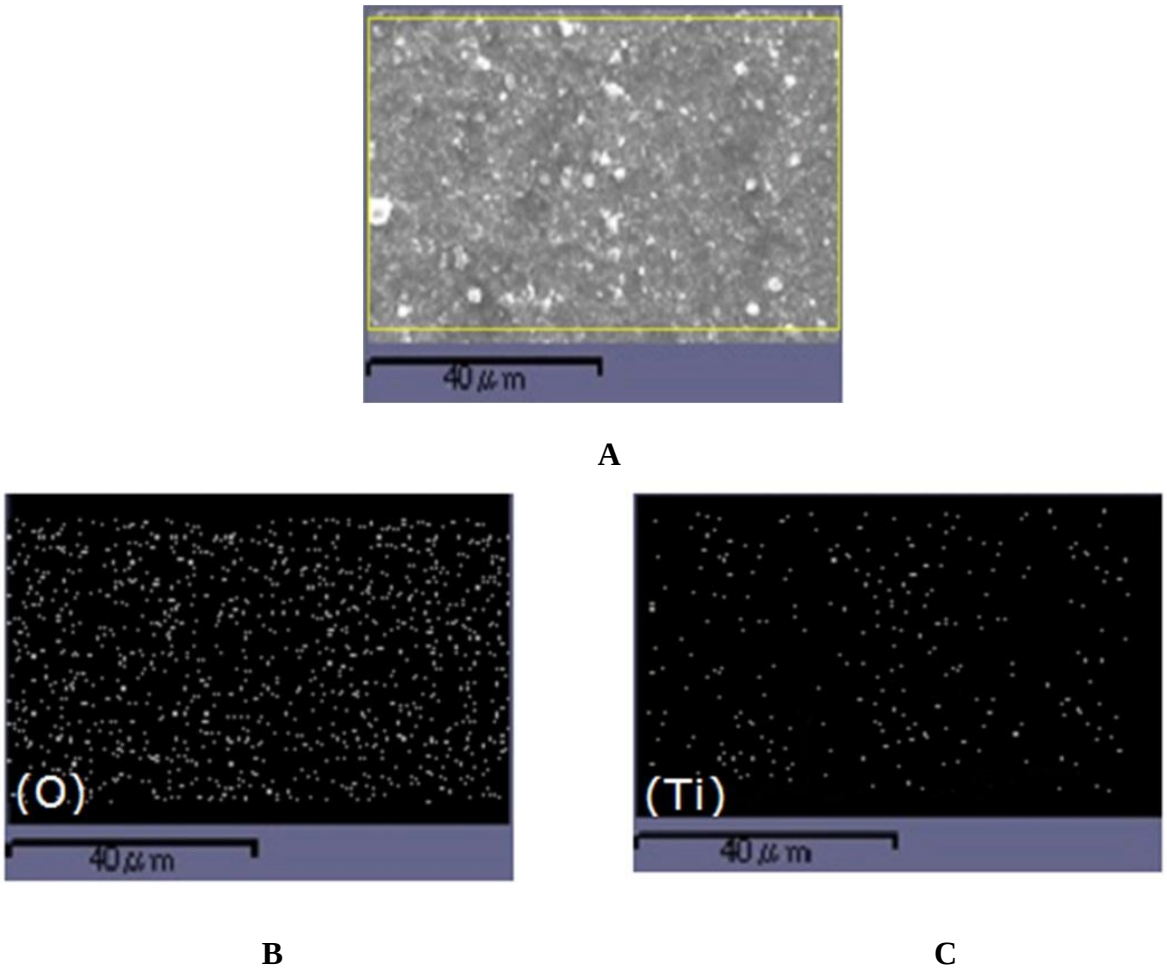

Figure 3. (a) SEM surface morphology, (b) O mapping, and (c) Ti mapping of electroless Ni-P/10 g/L TiO_2 composite coating.

Figure 4 presents the variation in the composition of the composite coatings. The amounts of O and Ti elements inthe composite coatings increase with the concentration of TiO_2 in the plating solution, providing evidence of an increase in the incorporation of nano-TiO_2 particles in the coating (Figs. 4a and 4b). Figures 4c and 4d reveal that the second-phase nano-TiO_2 particles in the Ni-P matrix influenced the co-deposition phosphorus, reducing the phosphorus content of 20.03 wt.% in the Ni-P coating to 8.35 wt.% in the Ni-P/nano-TiO_2 composite coating, which was formed when 15 g/L TiO_2 was added to the plating solution. This result is close to that of *Novakovic et al.* [17], who found that the incorporation of nanometer-sized TiO_2 particles affected the phosphorus content. A slight decrease in phosphorus content has been observed when the nano-TiO_2 particles were incorporated into an Ni-P matrix with a high phosphorus content [17]. The cross-sections of the coatings reveal that no interfacial void or defect is present between the coatings and the 70-30 brass substrate (Fig. 5). Additionally, the thickness of the nanocomposite coatings that is determined from their cross-sections substantially exceeds that of the Ni-P coating, and increases with the added TiO_2 concentration in the plating solution (Fig. 6). When the TiO_2 concentration is increased to 15 g/L, the average thickness of the Ni-P/nano-TiO_2 composite coating is approximately 7.82 μm, which is approximately three times

that of the electroless Ni-P coating (2.82 μm) that is deposited under the same conditions.

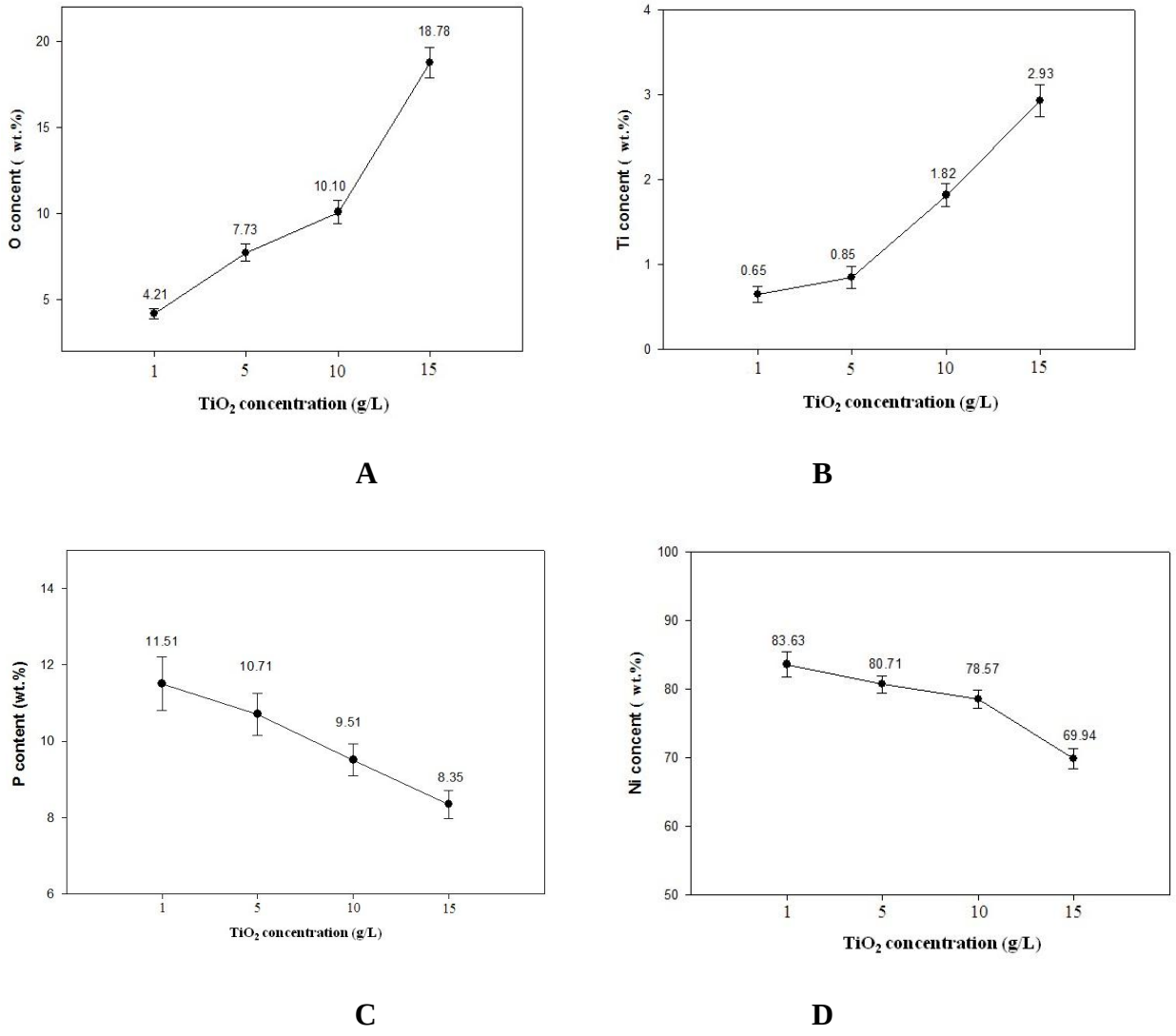

Figure 4. Elemental contents of electroless Ni-P/TiO_2 composite coatings as function of concentration of added TiO_2 in plating solution: (a) O (b) Ti (c) P (d) Ni.

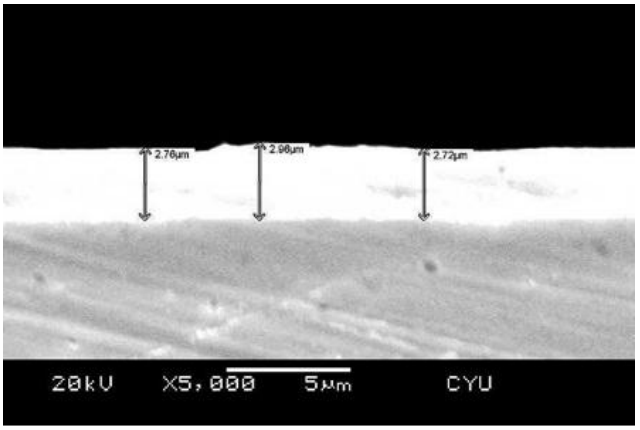

A

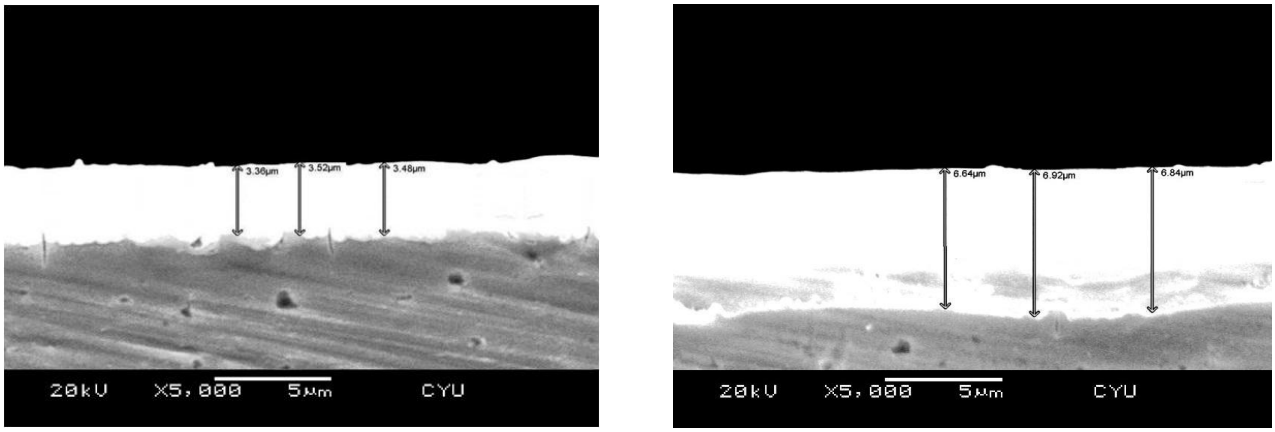

B **C**

Figure 5. SEM cross-sectional images and EDS elemental analysis of (a) electroless Ni-P coating, (b) electroless Ni-P/1 g/L TiO_2 composite coating and (c) electroless Ni-P/10 g/L TiO_2 composite coating.

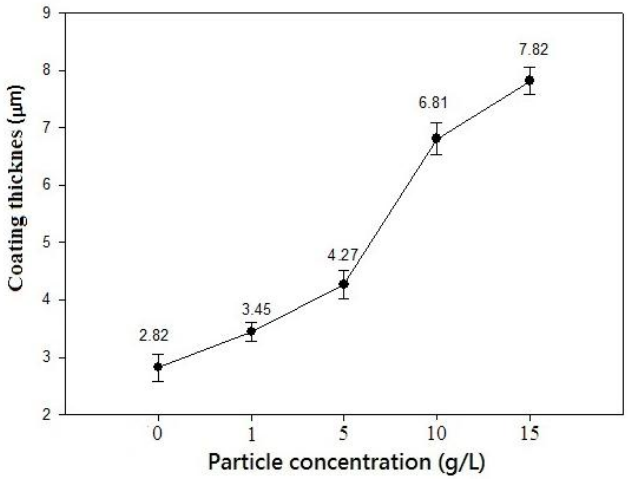

Figure 6. Average thickness of electroless Ni-P/TiO_2 composite coatings as function of concentration of added TiO_2 in plating solution.

Similar results have been obtained from electroless Ni-P/nano-SiO_2 composite coatings, and these can be explained by the fact that both TiO_2 and SiO_2 nanoparticles, which have large surface areas, high surface energies and activities can be easily adsorbed on initially reduced Ni particles and co-deposited on the substrate to increase the substrate activity, and thereby increasing the deposition rate [26]. Figure 7 presents the microhardness of the 70-30 brass substrate, electroless Ni-P and Ni-P/nano-TiO_2 coatings.

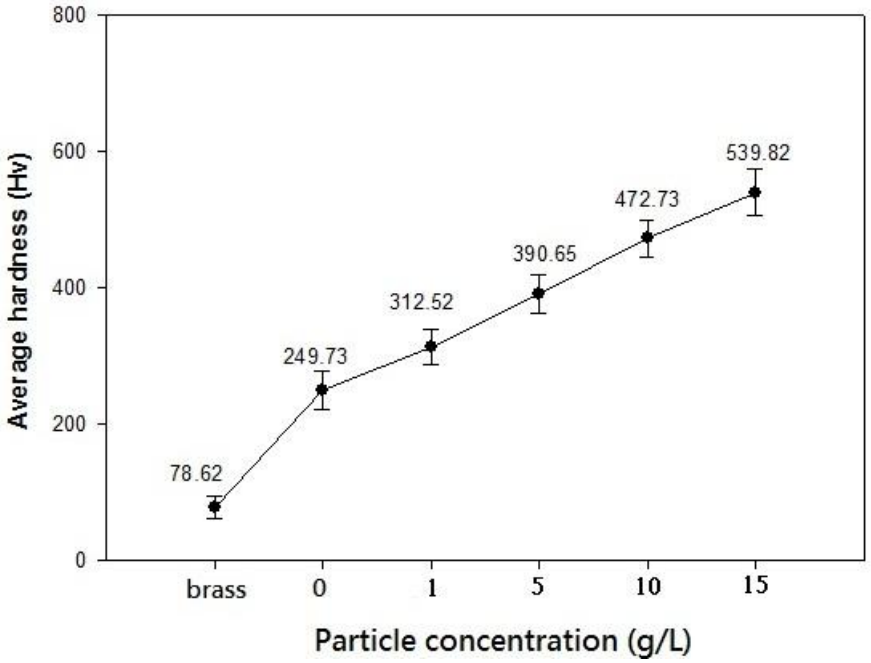

Figure 7. Microhardness of 70-30 brass substrate and electroless Ni-P/TiO_2 composite coating.

Generally, electroless Ni-P and Ni-P/nano-TiO_2 coatings that are plated on 70-30 brass substrate increase its microhardness. An electroless Ni-P coating with a phosphorus content that exceeds 8 wt.% has a high hardness because it is amorphous [25]. The Ni-P/nano-TiO_2 composite coatings in this study had a higher microhardness than the Ni-P coating. indicating that nano-TiO_2 particles that were codeposited in the composite coatings acted as barriers that retarded the plastic deformation of the Ni-P matrix and thereby increased the microhardness. Nano-TiO_2 particles as a second phase can reinforce the Ni-P matrix and impede the rapid propagation of dislocations in a ductile Ni-P matrix. This result is consistent with the finding that many hard nano-particles reinforce an electroless Ni-P matrix coating system [17-19,27-30]. Figures 6 and 7 show a good correspondence to each other. Thus, the increase in the hardness with the TiO_2 content in the coating solution may not be the property of the coating but the increase in thickness leads to a decrease in the influence of the softness of the substrate.

3.2. Electrochemical polarization testing

Figure 8 presents the potentiodynamic polarization curves of the 70-30 brass substrate, and electroless Ni-P and Ni-P/TiO_2 coatings in 0.1 M NaF solution. The electroless Ni-P and Ni-P/TiO_2 coatings had a more positive corrosion potential and lower anodic corrosion current density than the 70-30 brass substrate. Electroless Ni-P/TiO_2 coatings have a more noble character than the electroless Ni-P coating, consistent with their denser and finer structure than that of the Ni-P coating. The high corrosion resistance of the electroless Ni-P coating in this study was a result of its amorphous structure and nickel was preferentially dissolved at open circuit potential, increasing the amount of phosphorus

in the surface layer [24,31,32]. The surface that was enriched with phosphorus reacted with water to form a layer of adsorbed hypophosphite anions ($H_2PO_2^-$). This layer in turn blocked the supply of water to the surface of the electrode [33]. In the Ni-P/nano-TiO_2 composite coating, the TiO_2 particles formed a barrier by filling up the very small pores in the metal matrix, making the film more compact and minimizing the solution-metal interaction, potentially improving the corrosion resistance of the composite coating remarkably above that of a pure alloy coating. Although the corrosion resistance of the Ni-P/nano-TiO_2 composite coating increased with the concentration of nano-TiO_2 particles that were added to the plating solution, increasing that concentration to 15 g/L reduced the corrosion potential of the Ni-P/nano-TiO_2 coating and increased corrosion current density. This effect may be explained by worsening of the coating structure by cracking (Fig. 2d).

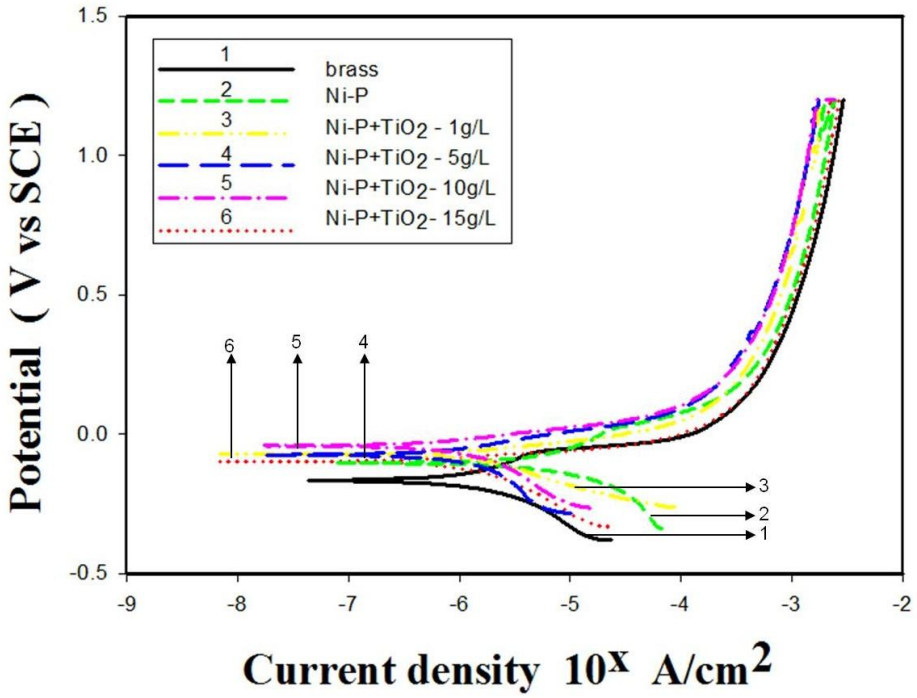

Figure 8. Potentiodynamic polarization curves of 70-30 brass substrate, electroless Ni-P coating and electroless Ni-P/TiO_2 composite coatings in 0.1 M NaF solution.

Figure 8 also reveals that the anodic polarization curve of the 70-30 brass substrate exhibited a weak passive characteristic. Although a passive film was formed, this passive film had a significant negative passive potential and low passive current density, implying that the passive film was unstable and easily broken, resulting in rapid anodic localized dissolution. This passive film is Cu_2O, as revealed by XRD [34], and the Cu_2O could be shown according to the potential-pH diagram for Cu/H_2O at 25 ˚C [35]. Theoretically, a brass alloy in fluoride solution is attacked by F^-, causing a corrosion reaction of copper, which proceeds by the direct oxidation and complexing of copper by the fluoride ions:

$$Cu + 2\ F^- \rightarrow CuF_2^- + e^- \quad (1)$$

(2) The Cu_2O surface film is then formed by hydrolysis of the CuF_2^- complex:

$$2\ Cu\ F_2^- + H_2O \rightarrow Cu_2O + 4\ F^- + 2\ H^+ \quad (2)$$

(3) Zinc is then dissolved following dezinfication from brass:

$$Zn \rightarrow Zn^{2+} + 2e^- \quad (3)$$

Since the XRD pattern included no signal from the fluoride compound of zinc [34], fluoride ions are assumed to attack the brass through Zn^{2+} to form soluble complexes [7]. Accordingly, the F^- ions can destroy the passive film Cu_2O and act as a catalyst that accelerates the preferential dissolution of zinc, producing a de-alloyed layer on the brass. These reactions can be described as follows.

$$Zn + 2\ F^- \rightarrow ZnF_2 + 2\ e^- \quad (4)$$

$$ZnF_2 \rightarrow Zn^{2+} + 2\ F^- \quad (5)$$

Although at a high TiO_2 concentration of 15 g/L, the Ni-P/nano-TiO_2 composite coating exhibits a slightly reduced corrosion resistance, it remains greater than that of the Ni-P coating. These results reveal the electroless Ni-P/nano-TiO_2 composite coating that was formed at a TiO_2 concentration of 10 g/L is the most effective for protecting 70-30 brass against corrosion in fluoride solution, as is consistent with its dense and fine microstructure (Fig. 2c) and high phosphorus content of approximately 9.51 wt.%. *Habazaki et al.* [36] found that amorphous Ni-P alloys with a phosphorus content of approximately 25 at.% had high corrosion resistance because they formed compact Ni3P films. In this study, the Ni-P coating had a phosphorus content of approximately 32 at.% and the Ni-P/nano-TiO_2 composite coating that was formed at a TiO_2 concentration of 10 g/L had a phosphorus content of approximately 16 at.%. These values sufficed for the initial preferential dissolution of nickel and the enrichment of the coating surface with phosphorus, which acted as a barrier to further dissolution. A comparison of the corrosion resistance of electroless Ni-P coating with that of Ni-P/nano-TiO_2 composite coatings revealed that the latter offered greater protection against corrosion. This result is reasonable, because even though the coatings have the same apparent area, the effective metallic area that is prone to corrosion is substantially lower in the case of the electroless composite coating. Additionally, nano-TiO_2 many micro-cells form facilitating anodic polarization and thereby inhibiting localized corrosion, such that mostly homogeneous corrosion occurs [37].

3.3. Slow strain rate tensile testing

Figure 9 plots the stress-strain curves for 70-30 brass substrate, and for electroless N-P and Ni-P/TiO_2 coatings following SSRT testing in 0.1 M NaF solution under the open circuit potential (OCP)

condition at a strain rate of 2.22×10^{-7} s^{-1}. The curves are similar to the conventionally shaped curves that are obtained for other alloys, and they are characterized by an increase of strain with stress up to the yield stress before slightly increasing untill it reaches a maximum, beyond which the strain begins to fall to the point of failure. Electroless Ni-P and Ni-P/ nano-TiO_2 composite coatings have a higher strain at failure. The SSRT was also performed in air to provide a standard of comparison, because the strain rate has no appreciable effect on tensile stress or ductility in air [22]. Figures 10a and 10b plot the ultimate tensile strength (UTS) and fracture strain (ε), respectively, that are obtained from the stress-strain curves of the specimens under OCP condition. The electroless Ni-P and Ni-P/nano-TiO_2 coatings clearly have a higher UTS and ε than the substrate, indicating that the protection of the 70-30 brass against SCC in fluoride solution. The ability of electroless Ni-P/nano-TiO_2 composite coating to protect against SCC is superior to that of the Ni-P coating, and is maximal (highest UTS and ε) when the concentration of added nano-TiO_2 is 10 g/L. When the added nano-TiO_2 concentration is increased over 10 g/L to 15 g/L, the UTS and ε of the formed composite coating slightly fall.

When the physically coated layer is present, the elongation in SSRT experiment will continue until the breakdown of the surface coating layer under the open circuit condition. Once the breakdown of the surface coating layer occurs stress assisted corrosion of the substrate metal occurs. Thus, the fracture strength of the specimens with the coated layers is longer than that of the 70-30 alloy. However, the fracture strength of the coated specimens did not show regular change because the SCC fracture strength is affected by the situation of breakdown of the surface coating layer. At least one can say that because of higher cathodic activity of the coated layer once the substrate alloy is exposed to the solution the corrosion of the substrate alloy is accelerated by the presence of the cathodically active coated layer. The fracture surface will be affected by the presence of precipitated TiO_2 particles.

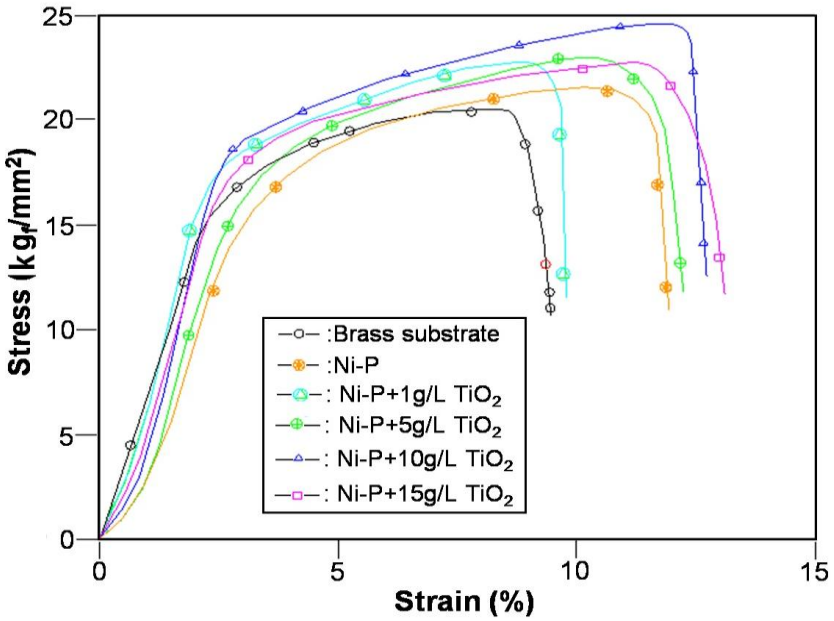

Figure 9. Stress-strain curves of 70-30 brass substrate, electroless Ni-P coating and electroless Ni-P/TiO_2 composite coatings following SSRT testing in 0.1 M NaF solution.

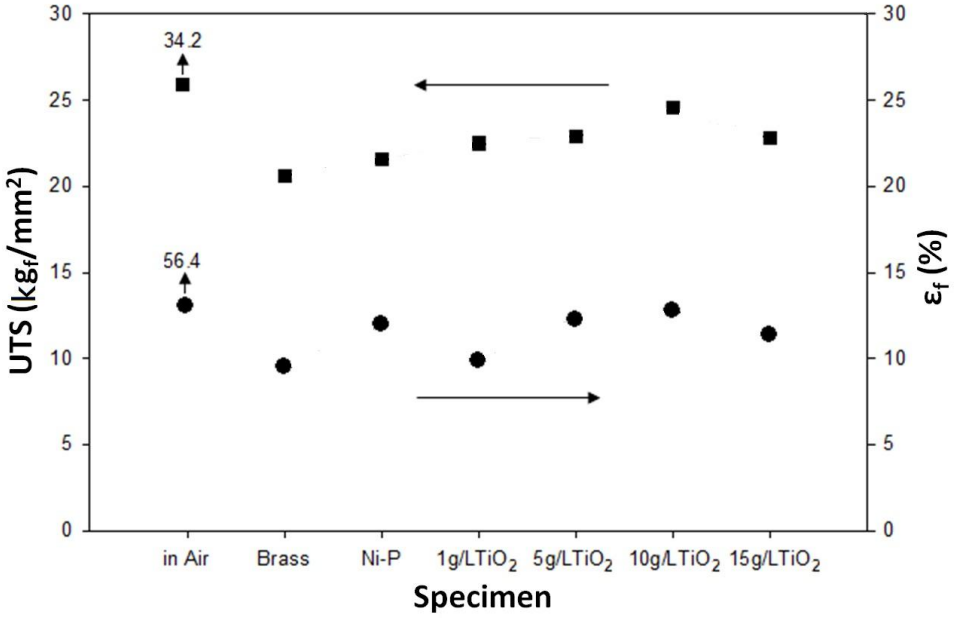

Figure 10. Variations in (a) UTS and (b) ε_f of the 70-30 brass substrate, electroless Ni-P coating and electroless Ni-P/TiO_2 composite coatings following SSRT testing in 0.1 M NaF solution.

Figures 11 a-g present the SEM fractographs of the fractured surfaces of the 70-30 brass substrates in air and in fluoride solution and of the coatings in fluoride solution. Figure 11a clearly reveals that the brass substrate sample in air has a dimpled fracture surface that is characteristic of completely ductile failure. The brass substrate in fluoride solution exhibits a cleavage fracture surface and intergranular cracking with characteristics of intergranular stress corrosion cracking (IGSCC) (Fig. 11b), The small strain at fracture verifies that the fracture is in a relatively brittle mode. SCC propagates mostly by active-path intergranular cracking. The cracks advance by preferential dissolution with the formation of active paths and stress concentrations at the tips of the cracks. The stress at the crack tips opens up the cracks and ruptures the unstable passive film, exposing fresh metal to the corrosive environment and accelerating dissolution as dislocations move out of the surface during slip steps [1]. A comaprison of this phenomenon with above results concerning the corrosion of brass by dezincification reveals that the IGSCC failure of 70-30 brass in fluoride solution may be attributed to film rupture [1,38]. Pickering and Byrne [39] showed that the preferential dissolution of Zn occurred more readily from stressed brass than from brass without stress. SCC process involves the preferential dissolution of zinc, which is promoted at the crack tips. Therefore, the inhibition of denzincification is supposed to inhibit the SCC process. The electroless Ni-P and Ni-P/nano-TiO_2 composite coating provides strong protection against corrosion without the formation of an unstable oxide film or localized denzicification, reducing the cleavage IGSCC. The fracture surfaces of such coatings become gradually rougher and are ductile (Figs. 11c-g). In particular, the fracture mode of the electroless Ni-P/nano-TiO_2 composite coating at a TiO_2 concentration of 10 g/L exhibits the completely ductile characteristic of dimpled fracture (Fig. 11f) consistent with its having the greatest

corrosion resistance as well as a dense and fine coating structure that incorporates the nano-TiO_2 particles.

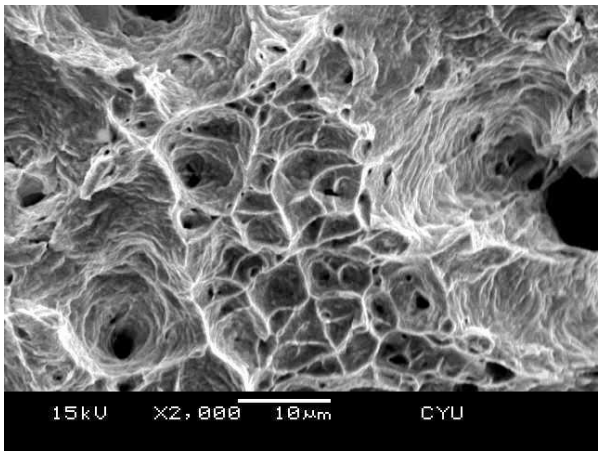

A

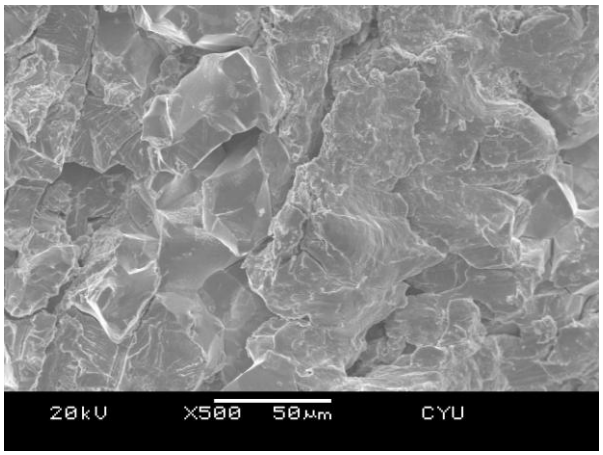

B

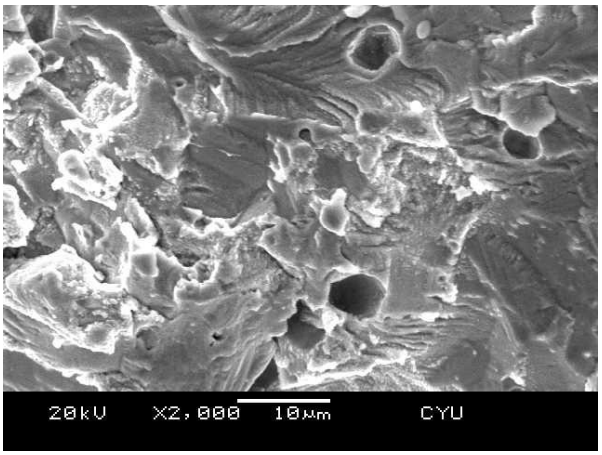

C

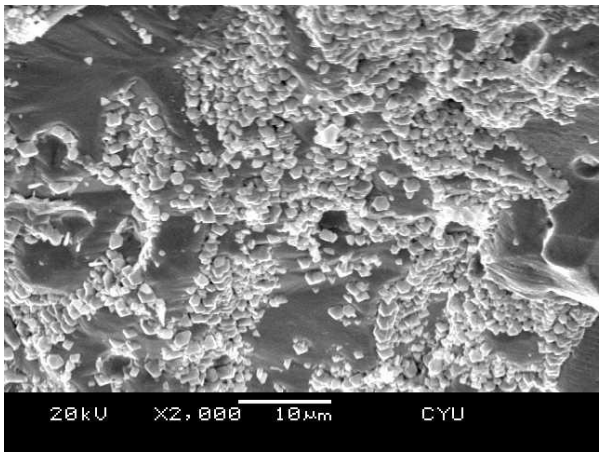

D

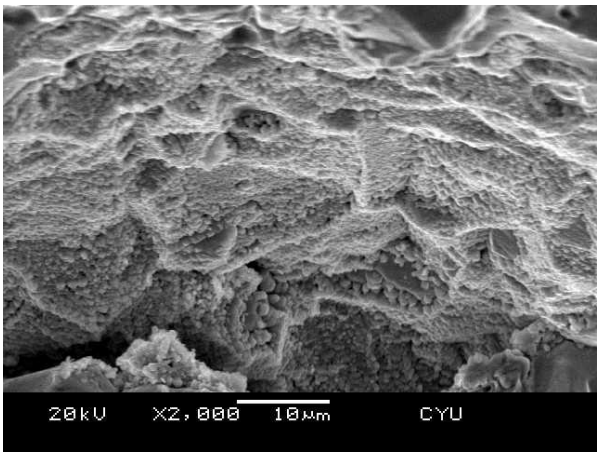

E

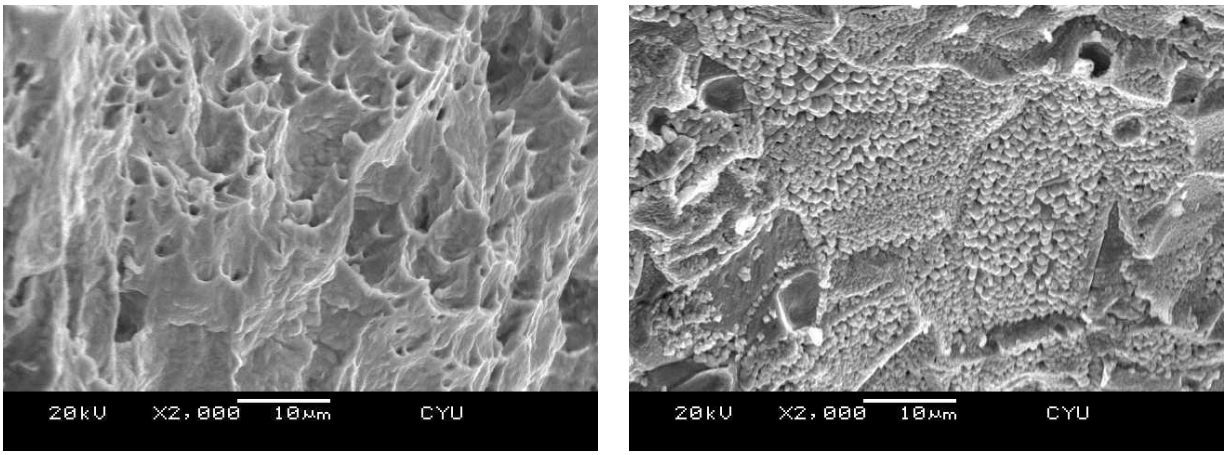

F **G**

Figure 11. SEM fractographs of fractured surfaces of (a) 70-30 brass substrate following SSRT testing in air, and of 70-30 brass substrate, electroless Ni-P coating and electroless Ni-P/TiO_2 composite coatings following SSRT testing in 0.1 M NaF solution: (b) 70-30 brass substrate (c) Ni-P, (d) N-P/1 g/L TiO_2, (e) Ni-P/5g/L TiO_2, (f) Ni-P/10g/L TiO_2 and (g) Ni-P/15g/L TiO_2.

4. CONCLUSIONS

(1) 70-30 Brass exhibited serious localized corrosion by dezincification and susceptibility to SCC in fluoride solution because of its weak passive behavior, which produced an unstable Cu_2O film, which was easily formed and broken down.

(2) A novel electroless Ni-P coating with a high P content of approximately 20 wt.% and electroless Ni-P/nano-TiO_2 composite coatings with high P contents (of over 8.35wt.%.) were uniformly deposited on 70-30 brass substrate.

(3) The amount of incorporated nano-TiO_2 increased with the concentration of nano-TiO_2 in the plating solution. The incorporation of nano-TiO_2 strengthened the Ni-P coating, and hardened the formed Ni-P/nano-TiO_2 composite coating to an extent that with the amount of nano-TiO_2 incorporated.

(4) The electroless Ni-P/nano-TiO_2 composite coating had a finer and denser coating structure than the Ni-P coating in fluoride solution, and the formed Ni-P/nano- TiO_2 composite coating retained a high phosphate content, which was responsible for their better electrochemical behavior and SCC susceptibility resistance. A nano-TiO_2 concentration of 10 g/L yielded the composite coating with the highest corrosion resistance and highest resistance to SCC. However, increasing the nano-TiO_2 concentration to 15 g/L reduced the corrosion resistance and SCC resistance by causing extensive aggregation and localized cracks.

(5) The electroless Ni-P/nano-TiO_2 composite coating favored anodic polarization and changed the localized active-passive transition to uniform corrosion behavior, owing to its high P content and incorporated nano-TiO_2. It therefore reduced susceptibility to SCC in flouride solution.

ACKNOWLEDGEMENTS
The author would like to thank the National Science Council of the Republic of China, Taiwan, for financially supporting this research under Contract No. NSC -100-2622-E-231-001-CC3.

References

1. T.K.G. Namboodhiri, R.S. Tripathi, *Corros. Sci*. 26 (1986) 745
2. R. Nishimura, T. Yoshida, *Corros. Sci*. 50 (2008) 1205
3. J. Yu, R.N. Parkins, *Corros. Sci*. 27 (1987) 159
4. G. Mori, D. Scherer, S. Schwentenwein, P. Warbichler, *Corros. Sci.* 47 (2005) 2099
5. A. Nagiub, F. Mansfeld, *Corros. Sci*. 43 (2001) 2147
6. C.K. Lee, H.C. Shih, *J. Electrochem. Soc*. 142 (1995) 731
7. H.C. Shih, R.J. Tzou, *J. Elecrochem.Soc*. 138 (1991) 985
8. H.C. Shih, R.J. Tzou, Y.N. Chen, Y.S. Lee, *Corrosion* 46 (1990) 913
9. H.C. Shih, R.J. Tzou, *Corros. Sci*. 35 (1993) 479
10. C. Subramanian, G. Gavallaro, G. Winkelman, *Wear* 241 (2000) 228
11. Y.J. Hu, L. Xiong, J.L. Meng, *Appl. Surf. Sci*. 253 (2007) 5029
12. C.M. Liu, W.L. Liu, S.H. Hsieh, T.K. Tsi, W.J. Chen, *Appl. Surf. Sci*. 243 (2005) 259
13. F.T. Chi, K. Jiang, B. Li, B. Jiang, *Appl. Surf. Sci*. 255 (2008) 2740
14. W.X. Zhang, N. Huang, J.G. He, Z.H. jiang, Q. Jiang, J.S. Lian, *Appl. Surf. Sci*. 253 (2007) 5116
15. C.K. Lee, *Mater. Chem. Phys*. 114 (2009) 125
16. K. Parker, H. Shah, *Plating* 58 (1971) 230
17. J. Novakovic, P. Vassiliou, K.I. Samara, Th. Argyropoulos, *Surf. Coat. Technol*. 201 (2006) 895
18. W. Chen, W. Gao, Y. He, *Surf. Coat. Technol*. 204 (2010) 2493
19. S. Ranganatha, T.V. Venkatesha, K. Vathsala, *Appl. Surf. Sci*. 256 (2010) 7377
20. ASTM G49-85, Preparation and use of direct tension stress corrosion test specimens, annual book of ASTM standards, Philadelphia, PA, 1982
21. D.A. Jones, Principles and Prevention of Corrosion, second ed., Prentice-Hall, 1996, p.265
22. S.A. Bradford, T. Lee, *Corrosion* 34 (1978) 96
23. S.S. Birley, D. Tromans, *Metall. Trans*. 12A (1981) 1215
24. I. Baskaran, T.S.N. Sankara Narayanan, A. Stephen, *Mater. Chem. Phys*. 99 (2006) 117
25. R.M. Abdel Hameed, A.M. Fekry, *Electrochim. Acta* 55 (2010) 5922
26. H.W. Xie, B.W. Zhang, *J. Mater. Process. Technol*. 124 (2002) 8
27. M. Novák, D. Vojtěch, T. Vitů, *Appl. Surf. Sci*. 256 (2010) 2956
28. F. Bigdeli, S.R. Allahkaram, *Mater. Des*. 30 (2009) 4450
29. C.M. Das, P.K. Limayer, A.K. Grover, A.K. Suri, *J. Alloys Compd*. 436 (2007) 328
30. J.T. Winowlin Jappes, B. Ramamoorthy, P. Kesavan Nair, *J. Mater. Process Technol*. 209 (2009) 1004
31. J.N. Balaraiu, T.S.N. Sankara Narayanan, S.K. Sesfadri, *J. Solid State Electrochem*. 5 (2001) 334
32. T. Rabizadeh, S.R. Allahkaram, A. Zarebidaki, *Mater. Des*. 31 (2010) 3174
33. J.N. Balaraju, V. Ezhil Selvi, V.K. Willium Grips, K.S. Rajam, *Electrochim. Acta* 52 (2006) 1064
34. Y.Y. Chen, R.J. Tzou, Y.S. Chang, L.H. Wang, J.C. Oung, H.C. Shih, *Corros. Sci*. 47 (2005) 79
35. M. Pourbaix, Atlas of Electrochemical Equilibria in Aqueous Solution, Pergamon press, London, 1974, p.171
36. H. Habazaki, Y.-P. Lu, A. Kawashima, K. Hashimoto, *Corros. Sci.* 32 (1991) 1227
37. A. Abdel Aal, *Mater. Sci. Eng*. A 474 (2008) 181
38. N.R. Smart, P.M. Scott, R.P.M. Procter, *Corros. Sci*. 30 (1990) 877
39. H.W. Pickering, P.J. Byrne, *Corrosion* 29 (1973) 325